J|A|C|S
ARTICLES
Published on Web 04/03/2004

Quantitative Evaluation of the Catalytic Activity of Dendrimers with Only One Active Center at the Core: Application to the Nitroaldol (Henry) Reaction

Aizpea Zubia, Fernando P. Cossío,* Iñaki Morao, Marina Rieumont, and Xabier Lopez*

Contribution from the Kimika Fakultatea, Euskal Herriko Unibertsitatea, P.K. 1072, 20080 San Sebastian-Donostia, Spain

Received December 1, 2003; E-mail: qopcomof@sq.ehu.es (F.P.C.); poplopex@sq.ehu.es (X.L.)

Abstract: One reference tertiary amine and three families of structurally related trialkylamines and dendrimers have been synthesized, characterized, and studied by molecular dynamics simulations. The catalytic activity of these amines in the nitroaldol (Henry) reaction between 2-nitroethanol and benzaldehyde has been measured by FT-IR spectroscopy. It is found that, in this kind of molecule with only one catalytic center at the core, the efficiency of the catalytic process decreases with the size and/or the degree of ramification of the dendrimer. According to these results, there is a linear departure from the behavior predicted by the hard sphere collision theory (HSCT) as the size of the dendrimer increases. Therefore, the behavior of structurally related dendrimers can be quantified in terms of their molecular weight and reagent accessible surfaces.

Introduction

The potential of dendritic molecules as catalysts was recognized almost since the beginning of this field of research.[1,2] In principle, one of the advantages of dendrimers in catalysis is the possibility of recovering the homogeneous catalytic macromolecule by microfiltration or precipitation. The second one consists of the possibility of developing tailor-made environments that, if appropriately designed, could produce results not affordable to low size analogues.

The design of dendritic catalysts offers multiple possibilities of installing the active centers. If the dendrimer incorporates only one catalytic point, this site can be at the core of the macromolecule[3] or it can occupy a focal point in a dendritic sector. Similarly, multiple catalytic centers can be incorporated inside the dendritic structures[3] or can be encapsulated without any covalent bond between the active sites and the macromolecule. Finally, the catalytic points can be installed on the periphery.[4]

Although the scope of reactions catalyzed by dendrimers is very large,[1−4] attempts to measure quantitatively the catalytic activity of different generations of dendrimers are very scarce to date. Thus, Chow et al.[5] have reported different selectivities and reaction rates in Diels Alder reactions catalyzed by bis(oxazoline)copper (II) dendrimers. These authors found that the formation constant of the dienophile−catalyst complex decreased gradually from the lower to the higher generations. In addition, the reaction rate constants remained essentially invariable from the zeroth to second generation, whereas it dropped suddenly for the third generation. This result was rationalized in qualitative terms by assuming that the size of the dendritic sectors in the bulkiest catalyst induces a change in the accessibility of the catalytic site. Similarly, Seebach et al.[6] found a slight decreasing of the catalytic activity of different TADDOL derivatives with the generation number in the diethyl zinc addition to benzaldehyde, with an abrupt variation for the bulkiest dendrimer. In the same vein, Diederich et al.[7] measured quantitatively a decay of the catalytic activity of dendritic thiazolio-cyclophanes in the course of the oxidation of naftalene-2-carboxaldehyde. More recently, Astruc et al. have observed negative dendritic effects in the catalysis of the Sonogashira reaction between terminal alkynes and vinyl halides[8] and in the ring opening metathesis polymerization of norbornene.[9]

Quantitative measurement of positive dendritic effects in catalysis is also scarce. For example, Detty et al. have reported an increasing activity per peripheric catalytic site in the oxidation of bromide by hydrogen peroxide.[10] In a related approach, Twyman and Martin[11] measured a 25-fold rate enhancement in the aminolysis of *p*-nitrophenyl acetates with a PAMAM

(1) (a) Astruc, D.; Chardac, F. *Chem. Rev.* **2001**, *101*, 2991. (b) Janssen, H. M.; Meijer, E. W. *Chem. Rev.* **1999**, *99*, 1665. (c) Newkome, G. R.; He, E.; Moorefield, C. N. *Chem. Rev.* **1999**, *99*, 1689. For seminal contributions in this field, see, inter alia: (d) Knapen, J. W. J.; van der Made, A. W.; de Wilde, J. C.; van Leeuwen, P. W. N. M.; Wijkens, P.; Grove, D. M.; van Koten, G. *Nature* **1994**, *372*, 659. (e) Brunner, H.; Fürst, S. *Tetrahedron* **1994**, *50*, 4303. (f) Brunner, H. J. *Organomet. Chem.* **1995**, *500*, 39.

(2) (a) Hecht, S.; Fréchet, J. M. J. *Angew. Chem., Int. Ed.* **2001**, *40*, 74. (b) Oosterom, G. E.; Reek, J. N. H.; Kamer, P. C. J.; van Leeuwen, P. W. N. M. *Angew. Chem., Int. Ed.* **2001**, *40*, 1828.

(3) Twyman, L. J.; King, A. S. H.; Martin, I. K. *Chem. Soc. Rev.* **2002**, *31*, 69.

(4) (a) Reek, J. N. H.; de Groot, D.; Oosterom, G. E.; Kamer, P. C. J.; van Leeuwen, P. W. N. M. *Rev. Mol. Biotechnol.* **2002**, *90*, 159. (b) van Koten, G.; Jastrzebski, J. T. B. H. *J. Mol. Catal. A* **1999**, *146*, 317.

(5) (a) Mak, C. C.; Chow, H.-F. *Macromolecules* **1997**, *30*, 1228. (b) Chow, H.-F.; Mak, C. C. *J. Org. Chem.* **1997**, *62*, 5116.

(6) Rheiner, P. B.; Seebach, D. *Chem.−Eur. J.* **1999**, *5*, 3221.

(7) Habicher, T.; Diederich, F.; Gramlich, V. *Helv. Chim. Acta* **1999**, *82*, 1066.

(8) Heuzé, K.; Méry, D.; Gauss, D.; Astruc, D. *Chem. Commun*. **2003**, 2274.

(9) Gatard, S.; Nlate, S.; Cloutet, E.; Bravic, G.; Blais, J.-C.; Astruc, D. *Angew. Chem., Int. Ed.* **2003**, *42*, 452.

(10) Francavilla, C.; Bright, F. V.; Detty, M. R. *Org. Lett.* **1999**, *1*, 1043.

10.1021/ja039888s CCC: $27.50

dendrimer with respect to an equivalent amount of *N*-acetyl ethylenediamine. Alternatively, Fréchet et al. proposed a different strategy based upon the installation of a catalytic center at the core of the dendrimer and on the generation of an inside−outside polarity gradient. This favors the interaction between the reactants and the catalytic center and prevents product inhibition of the active site. This strategy to generate positive dendritic effects proved to be successful in the conversion of cyclopentadiene to *cis*-2-cyclopentene-1,4-diol catalyzed by dendritic ambiphilic singlet oxygen sensitizers.[12] In this case, the gradient was established between an hydrophobic core and a polar environment. An inverse design was also successful in the catalysis of E1-type[13] and esterification reactions.[14] Finally, a very recent paper of Liu and Breslow[15] reports quantitative measurements of large rate enhancements in the catalytic transamination of piruvic and phenylpiruvic acids by PAMAM dendrimers incorporating one pyridoxamine unit at the core.

Our group[16] reported that dendrimers derived from triethylamine catalyze the nitroaldol (Henry) reaction. Similarly, Smith et al.[17] found that dendrimers containing a tertiary amine and dendritic branches derived from L-lysine catalyze the same reaction. In both cases, the activity of the catalysts decreased with the generation number, in agreement with most of the above-mentioned results.

In all these precedents the description of the features of the different generations of catalysts was based upon plausible and qualitative arguments. Within this context, we decided to study the possibility of correlating the kinetic behavior of one family of structurally related dendritic catalysts with some of their structural parameters. This correlation could eventually help in the design of other catalysts. To facilitate the study, we designed our dendritic catalysts taking into account the following requirements: (i) one single and structurally simple catalytic center at the core, (ii) highly symmetric branches and periphery, and (iii) different branching indexes and generations without significant changes in the neighborhood of the catalytic site.

Therefore, the aim of the present work has been to measure the catalytic activity of structurally related triethanolamine-derived dendrimers with different generation numbers and branching indexes, in an attempt to correlate the catalytic activity with different parameters of the dendritic molecules. As we did in our previous work,[16] the reaction studied is the nitroaldol (Henry) reaction, which can be catalyzed by amines.[18]

Results and Discussion

Chemical Synthesis of the Catalysts. All the catalysts prepared were based on the methodology reported in our previous work,[16] but incorporated different branching units. Thus, around a single catalytic center at the core (a nitrogen atom) surrounded by a common triethanol moiety, different generations of substituted benzyloxy units were incorporated

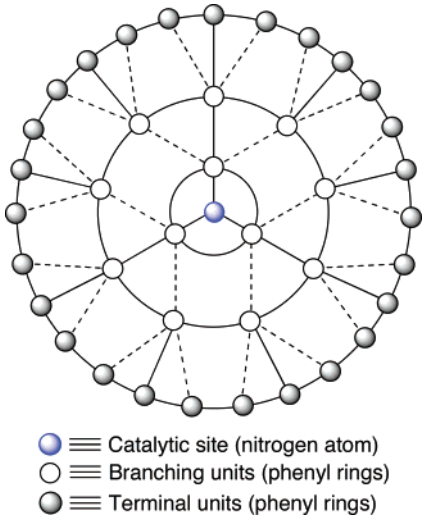

Figure 1. Basic features of dendrimers designed for the catalysis of the nitroaldol (Henry) reaction. Lines connecting the branching and terminal units are alkoxylidene groups.

(Figure 1). In all of these tertiary amines, terminal benzyloxy groups provided a common hydrophobic periphery.

In all cases, the synthesis of the catalyst was accomplished by Williamson reaction between triethanolamine **1** and different benzyl bromides (Schemes 1−3). In the simplest case, the tribenzyloxyethylamine **A0** was obtained in 61% yield after 24 h of reaction at room temperature in the presence of 3 equiv of benzyl bromide. The synthesis of the linear congener **MA1** was accomplished in 75% yield after 48 h of reaction at room temperature. Similarly, the second-generation analogue **MA2** was obtained in 53% yield under the same reaction conditions. Bromides **2** and **3** (Scheme 1) were readily prepared using the hydroxy benzylic alcohol strategy developed by Fréchet[19] (see Supporting Information).

The synthesis of dendrimers **DA1** and **DA2** was carried out in the same way from **1** and bromides[19] **4** and **5** (Scheme 2). As in the monosubstituted series, the yield of the second-generation dendrimer **DA2** was lower than that obtained for its first-generation congener **DA1**. The reaction times required for these yields were 72 and 48 h, respectively.

Dendrimers **TA1** and **TA2** were prepared in the same way from **1** and bromides **6** and **7**, respectively. These halides were prepared in turn following the methodology developed by Fréchet and using the starting materials reported by Percec[20] (Scheme 3). To improve the yield of the last Williamson reaction, we used the bromides instead of the chlorides used by Percec et al.[20] in the synthesis of these 3,4,5-trisubstituted benzyl halides. The full details of the preparation and characterization of **6** and **7** are reported in the Supporting Information.

The characterization of these triethanolamine-derived dendrimers showed the different dynamic properties of these compounds depending on the generation number and/or the branching index. Thus, the nonaromatic region of their ^{1}H NMR spectra shows a progressive broadening of the two triplets corresponding to the ethylene moieties surrounding the catalytic centers (see Supporting Information). Similarly, the intensities

(11) Twyman, L. J.; Martin, I. K. *Tetrahedon Lett.* **2001**, *42*, 1123.
(12) Hecht, S.; Fréchet, J. M. J. *J. Am. Chem. Soc.* **2001**, *123*, 6959.
(13) Piotti, M. E.; Rivera, F.; Bond, R.; Hawker, C. J.; Fréchet, J. M. J. *J. Am. Chem. Soc.* **1999**, *121*, 9471.
(14) Liang, C. O.; Helms, B.; Hawker, C. J.; Fréchet, J. M. J. *Chem. Commun.* **2003**, 2524.
(15) Liu, L.; Breslow, R. *J. Am. Chem. Soc.* **2003**, *125*, 12110.
(16) Morao, I.; Cossío, F. P. *Tetrahedron Lett.* **1997**, *38*, 6461.
(17) Davis, A. V.; Driffield, M.; Smith, D. K. *Org. Lett.* **2001**, *3*, 3075.
(18) (a) Luzzio, F. A. *Tetrahedron* **2001**, *57*, 915. (b) Rosini, G. In *Comprehensive Organic Synthesis*; Trost, B. M., Ed.; Pergamon: New York, 1991; Vol. 2, pp 321−340.
(19) (a) Hawker, C. J.; Fréchet, J. M. J. *J. Am. Chem. Soc.* **1990**, *112*, 7638. (b) Hawker, C. J.; Fréchet, J. M. J. *J. Chem. Soc., Chem. Commun.* **1990**, 1010.
(20) (a) Balagurusamy, V. S. K.; Ungar, G.; Percec, V.; Johansson, G. *J. Am. Chem. Soc.* **1997**, *119*, 1539. (b) Percec, V.; Cho, W. D.; Mosier, P. E.; Ungar, G.; Yeardley, D. J. P. *J. Am. Chem. Soc.* **1998**, *120*, 11061.

Scheme 1. Synthesis of Amines **A0**, **MA1**, and **MA2**[a]

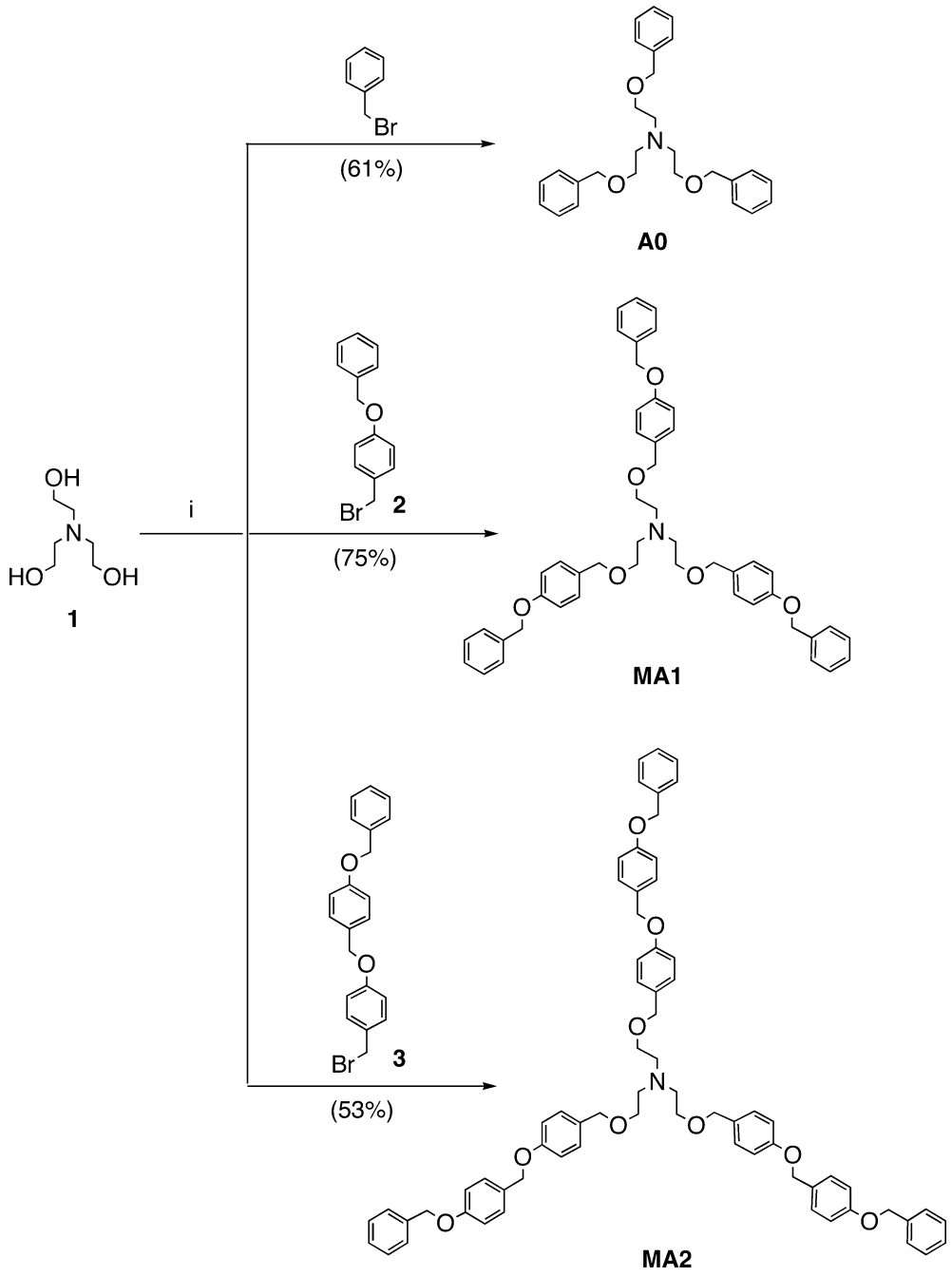

[a] Reagents and conditions: (i) NaH (3.2 equiv), RBr (3.2 equiv), THF/DMF, room temperature.

and the chemical shifts of the different benzyl methylene groups permitted in most cases the assignation of the different signals.

Measurement of the Catalytic Activity. The model reaction to study the catalytic power of our dendrimers was the Henry reaction between benzaldehyde **8** and nitro ethanol **9** to yield nitroaldols *syn*- and *anti*-**10** (Scheme 4). Given that the mechanism of this reaction consists of multiple steps,[18,21] kinetic treatment by means of an analytic rate equation is very complicated and difficult to analyze. To overcome this drawback, we decided to work under pseudo-first-order conditions, with a large excess of **9**.[22] Therefore, we measured the disappearance of **8** according to eq 1, where k_{obs} is the observed rate coefficient.

$$-\frac{d[\mathbf{8}]}{dt} = k_{obs}[\mathbf{8}] \quad (1)$$

Experimentally, we monitored the IR signal corresponding to the carbonyl group of **8** as it is shown in Figure 2A, using the stretching vibration of the C−N triple bond of benzonitrile as internal standard (see Supporting Information). Therefore, after measuring carbonyl absorbances at different times, we used the following expression to calculate k_{obs}:

$$\ln(A_t - A_\infty) = \ln(A_0 - A_\infty) - k_{obs}t \quad (2)$$

(21) Lecea, B.; Arrieta, A.; Morao, I.; Cossío, F. P. *Chem.−Eur. J.* **1997**, *3*, 20.
(22) Steindfeld, J. I.; Francisco, J. S.; Hase, W. L. *Chemical Kinetics and Dynamics*; Prentice Hall: Upper Saddle River, NJ, 1999; pp 40−41.

Scheme 2. Synthesis of Amines **DA1** and **DA2**[a]

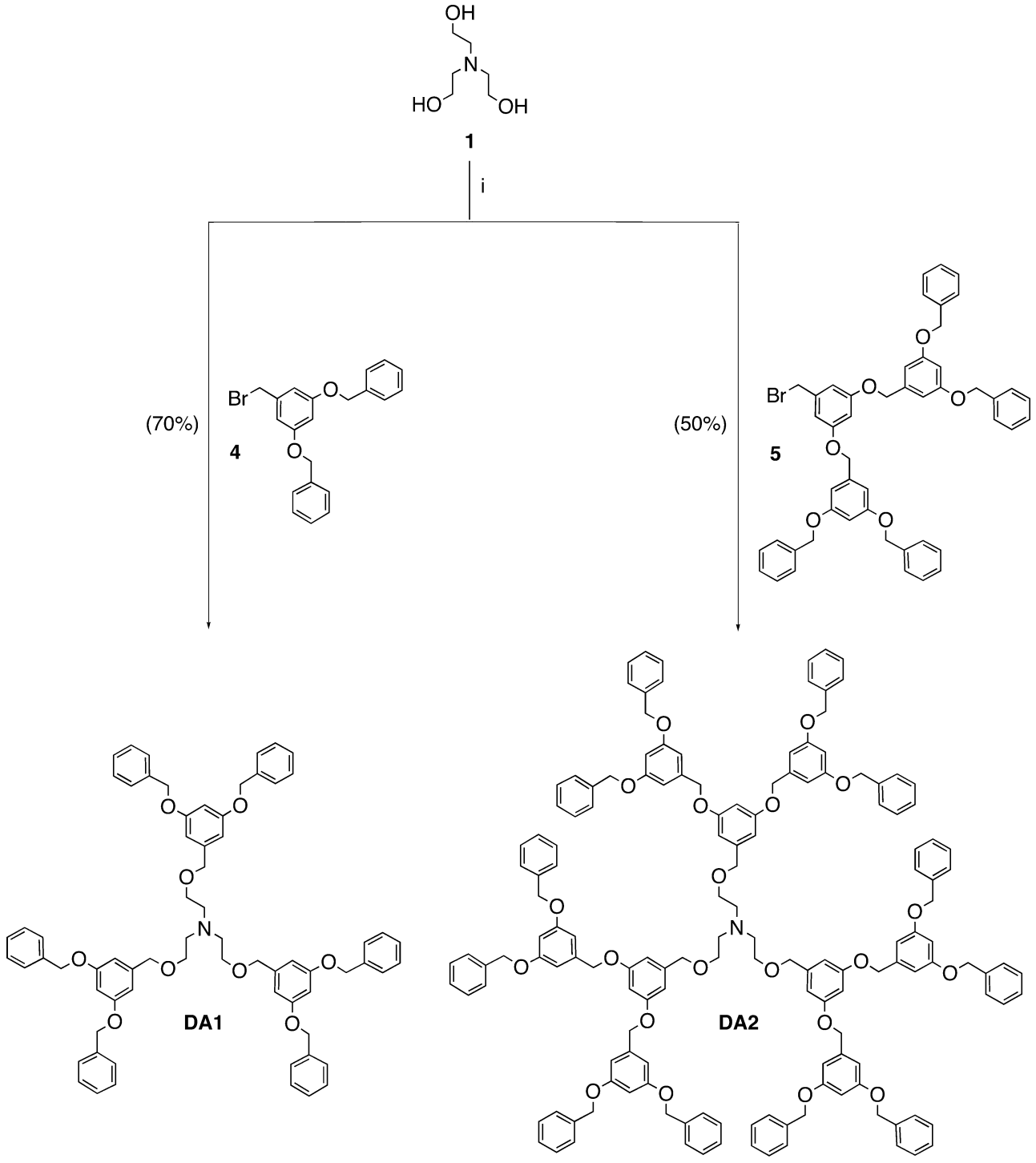

[a] Reagents and conditions: (i) NaH (3.2 equiv), RBr (3.2 equiv), THF/DMF, room temperature.

where A_0, A_t, and A_∞ indicate initial absorbance and absorbancies at times t and ∞, respectively. Given that the direct measurement of A_∞ is difficult and not reliable, we used the Kezdy–Swinbourne method to estimate it.[23,24] According to this method, absorbancies at times t and $t + \tau$ can be written in the forms

$$A_t = (A_0 - A_\infty) \exp(-k_{obs}t) + A_\infty \quad (3)$$

$$A_{t+\tau} = (A_0 - A_\infty) \exp[-k_{obs}(t + \tau)] + A_\infty \quad (4)$$

Dividing eqs 3 and 4 and solving for A_t leads to the following expression:

$$A_t = A_\infty[1 - \exp(k_{obs}\tau)] + A_{t+\tau} \exp(k_{obs}\tau) \quad (5)$$

Since the first term on the right of eq 5 is time independent, a plot of A_t versus $A_{t+\tau}$ will be linear, with a slope of $\exp(k_{obs}\tau)$. In addition, since at $t = \infty$ $A_t = A_{t+\tau}$, intersection of this line with the 45° line yields the value of A_∞, which can be used to calculate k_{obs} from eq 2. As an example, in Figure 2B,C we have included the results of one series of experiments involving the reaction depicted in Scheme 4 with **TA2** as catalyst. As it

Scheme 3. Synthesis of Amines **TA1** and **TA2**[a]

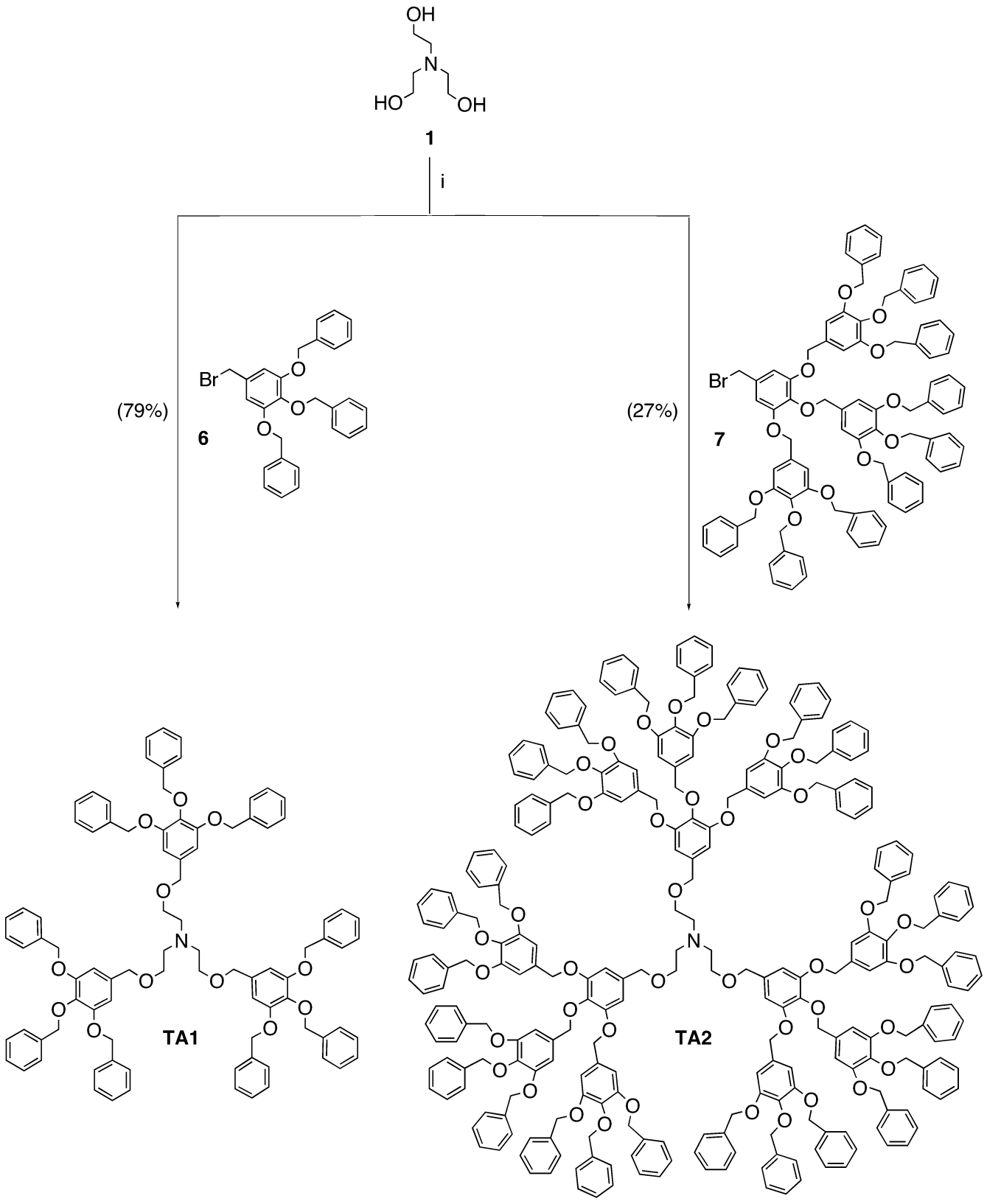

[a] Reagents and conditions: (i) NaH (3.2 equiv), RBr (3.2 equiv), THF/DMF, room temperature.

can be seen, under our experimental conditions, the reaction follows pseudo-first-order kinetics, with good linear correlations in both the A_t vs $A_{t+\tau}$ and $\ln(A_t - A_\infty)$ vs t representations. The same behavior was observed in the seven series of experiments involving catalysts described in Schemes 1−3. The observed rate coefficients are displayed in Table 1. In this table we have also included the stereochemical outcome of these reactions. According to our results, we have obtained a syn:anti ratio of ca. 2:1 in all cases, except when **TA2** was used as catalyst, in which the syn:anti ratio was slightly higher (2.6:1). The

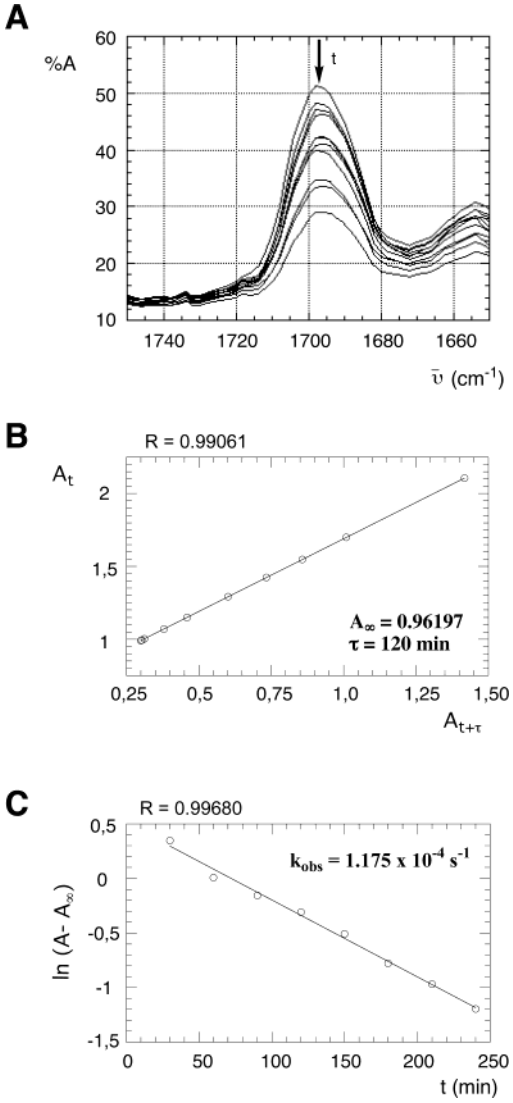

Figure 2. (A) FT-IR spectra of the carbonyl region of benzaldehyde at different reaction times corresponding to the reaction between benzaldehyde and nitroethanol catalyzed by dendrimer **TA2**. The arrow indicates the loss in absorbance at increasing reaction times. (B) Absorbances at times t and $t + \tau$ (A_t and $A_{t+\tau}$, respectively, with $\tau = 120$ min) for the same reaction. Intersection of the line with the 45° line yields the calculated A_∞ value (see text). (C) $\ln(A-A_\infty)$ versus time representation of the values measured for the same reaction under pseudo-first-order conditions.

Scheme 4. Nitroaldol Reaction between Benzaldehyde and Nitroethanol Catalyzed by Amines **A0**, **MA1-2**, **DA1-2**, and **TA1-2**

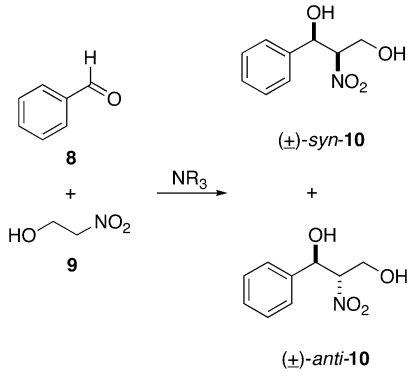

structural assignment of compounds **10** was made by comparison of our ^{1}H NMR data and those reported by Eyer and Seebach[25] (Scheme 4). Therefore, as an extension of our preliminary study involving only **A0**, **DA1**, and **DA2** compounds, we conclude that in our series of benzyloxy-based catalytic dendrimers neither the generation number nor the branching index has any significant impact on the stereocontrol of the reaction.

Table 1. Pseudo-First-Order Rate Coefficients (k_{obs})[a,b] for the Reaction between Benzaldehyde **8** and Nitroethanol **9** To Yield Racemic *syn*- and *anti*-2-Nitro-1-phenyl-1,3-propanediol **10**[c] (Scheme 4)

catalyst	k_{obs} (10^{-4} s^{-1})	syn/anti
A0	12.11 (±0.25)	66:34
MA1	10.85 (±0.34)	69:31
MA2	5.53 (±0.31)	67:33
DA1	8.25 (±0.62)	68:32
DA2	3.70 (±0.15)	66:34
TA1	1.89 (±0.43)	67:33
TA2	1.03 (±0.14)	72:28

[a] Calculated from FT-IR data by means of eqs 2 and 5. [b] Numbers in parentheses correspond to standard deviation from the average value. Each series of experiments was carried out in triplicate. [c] Determined by ^{1}H NMR in the crude reaction mixtures (see refs 16 and 25).

Computation of Structural Parameters of Catalysts. To gain a better understanding on the behavior of the dendrimers previously reported, we carried out several calculations of structurally significant parameters. All these computational studies were based upon molecular dynamics (MD)[26] and used the MM3 method[27] developed by Allinger et al. as implement in the *MacroModel*[28] package. To account partially for the solvent effects,[29] a dielectric constant of $\epsilon = 4.89$ was introduced, within a Born-generalized model for the electrostatic contribution to solvation energy and a solvent accessible surface (S_{AS})-based computation of the cavitation energy.[30] Therefore, this treatment does not account for specific solvent effects such as hydrogen bonds. The value of ϵ was chosen to account for a low polarity dielectric medium, representative in average of a mixture formed by the reactants and the hydrophobic branches of the dendrimer. All MD simulations were performed with SHAKE[31] to constrain the C−H bonds. The temperature was set up to 298 K. The system was equilibrated for 1 ns with time steps of 1 fs. This equilibration time is 10 times longer than the expected value for the relaxation time of dendrimers of this size.[32a] The production run was started from this point and lasted another nanosecond with time steps of 1 fs. In all cases, we observed that during the production period, the energy

(23) Espenson, J. H. *Chemical Kinetics and Reaction Mechanisms*; McGraw-Hill: New York, 1981; pp 24−30.
(24) (a) Kezdy, F. J.; Kaz, J.; Bruylants, A. *Bull. Soc. Chim. Belg.* **1958**, *67*, 687. (b) Swinbourne, E. S. *J. Chem. Soc.* **1960**, 2371.
(25) Eyer, M.; Seebach, D. *J. Am. Chem. Soc.* **1985**, *107*, 3601.
(26) (a) Haile, J. *Molecular Dynamics Simulations*; Wiley: New York, 1992. (b) Cramer, C. J. *Essentials of Computational Chemistry*; Wiley: Chichester, U.K., 2002; pp 63−94 and references therein.
(27) (a) Bowen, J. P.; Allinger, N. L. In *Reviews in Computational Chemistry*; Lipkowitz, K. B.; Boyd, E. D., Eds.; VCH Publishers: New York, 1991; Vol. 2, pp 81−97. (b) Allinger, N. L.; Yuh, Y. H.; Lii, J.-H. *J. Am. Chem. Soc.* **1989**, *111*, 8551. (c) Lii, J.-H.; Allinger, N. L. *J. Am. Chem. Soc.* **1989**, *111*, 8576.
(28) (a) *MacroModel*, version 7.0; Schrödinger: Portland, OR. (b) Mohamadi, F.; Richards, N. G. J.; Guida, W. C.; Liskamp, R.; Lipton, M.; Caulfield, C.; Chang, G.; Hendrickson, T.; Still, W. C. *J. Comput. Chem.* **1990**, *11*, 440.
(29) For related studies showing the importance of solvent effects on the conformation of dendrimers, see for example: (a) Hecht, S.; Vladimirov, N.; Fréchet, J. M. J. *J. Am. Chem. Soc.* **2001**, *123*, 18. (b) Chai, M.; Niu, Y.; Youngs, W. J.; Rinaldi, P. L. *J. Am. Chem. Soc.* **2001**, *123*, 4670.
(30) Still, W. C.; Tempczyk, A.; Hawley, R. C.; Hendrickson, T. *J. Am. Chem. Soc.* **1990**, *112*, 6127.
(31) Rickaert, J. P.; Ciccotti, G.; Berendsen, H. J. C. *J. Comput. Phys.* **1977**, *23*, 327.

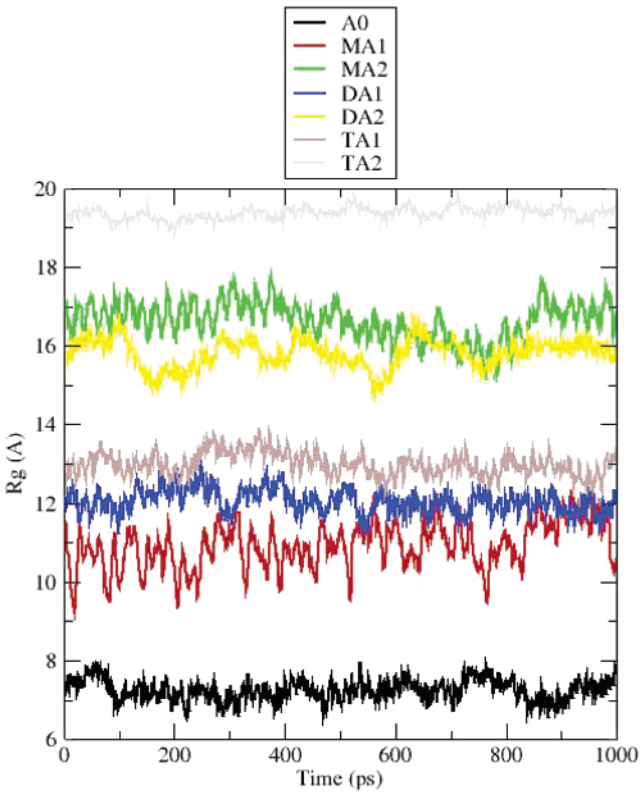

Figure 3. Evolution of the radius of gyration (R_g, in Å) along the production time of molecular dynamics simulations on catalysts **A0**, **MA1-2**, **DA1-2**, and **TA1-2**.

and temperature of the whole system were equilibrated.[32] During the production run, the coordinates were saved each picosecond, which implies a total of 1000 structures. These structures were used to calculate the averages of the properties specified below. To calculate these properties, programs based on the DYNAMO library[33] were written.

The first property computed from our MD data was the radius of gyration R_g, whose norm is given by[34]

$$R_g = \left[\frac{\sum_{i=1}^{N} m_i(\mathbf{r}_i - \mathbf{g})(\mathbf{r}_i - \mathbf{g})}{\sum_{i=1}^{N} m_i} \right]^{1/2} \quad (6)$$

where m_i is the mass of atom i ($i = 1,2...N$), $\mathbf{r}_i$ is its position vector, and $\mathbf{g}$ is the position vector of the center of masses:

$$\mathbf{g} = \frac{\sum_{i=1}^{N} m_i \mathbf{r}_i}{\sum_{i=1}^{N} m_i} \quad (7)$$

In Figure 3, we report the fluctuation of the R_g values for dendrimers **A0**, **MA1-2**, **DA1-2**, and **TA1-2** during the production time. As can be seen, the fluctuation of R_g obtained for the **MA1-2** dendrimers is considerably larger than that obtained for the more rigid compound **TA2**, which has a larger atom density at the periphery.

The square of the radius of gyration is related to the trace of the diagonalized tensor of inertia $\mathbf{I}_D$ of the molecule by means of the following expression:

$$tr(\mathbf{I}_D) = tr \begin{pmatrix} ML_1^2 & 0 & 0 \\ 0 & ML_2^2 & 0 \\ 0 & 0 & ML_3^2 \end{pmatrix} = MR_g^2 \quad (8)$$

As a convention, the components L_i are taken to satisfy the following expression:

$$L_1^2 > L_2^2 > L_3^2 \quad (9)$$

To correlate the shape of a given dendrimer with these magnitudes, it is useful to define the asphericity b in the form[35]

$$b = L_1^2 - \frac{1}{2}(L_2^2 + L_3^2) \quad (10)$$

Thus, b is related to the anisotropy of the molecule with respect to the principal axes. For a perfect sphere, $L_1 = L_2 = L_3$, and therefore $b = 0$.

Similarly, acylindricity c can be defined as[35]

$$c = L_2^2 - L_3^2 \quad (11)$$

Therefore, for a perfect cylinder, $L_2 = L_3$ and $c = 0$.

To interpret the structural data obtained for dendrimers **A0**, **MA1-2**, **DA1-2**, and **TA1-2**, we compared these data with those computed for three reference molecules (see Table 1 of the Supporting Information). These molecules are *n*-pentane, neopentane (2,2-dimethylpropane), and hexaethynyl benzene as examples of linear chain, spheric globular molecule, and star-disk structures, respectively. In addition, we also computed the maximum radius (R_{max}) of these molecules, defined as the maximum distance from the central nitrogen atom to the most distant atom:

$$\langle R_{max} \rangle = \langle \max |\mathbf{r}_N - \mathbf{r}_i| \rangle \quad (12)$$

where $\mathbf{r}_N$ and $\mathbf{r}_i$ are the position vectors of the nitrogen and the i atom. These data are reported in Table 2.

According to our results, the radii of gyration grow according to the generation and/or the branching numbers, whereas the averaged $\langle R_{max} \rangle$ values are almost constant for each generation, irrespective of the degree of branching. To facilitate the visualization of the shape of dendrimers **A0**, **MA1-2**, **DA1-2**, and **TA1-2**, we report in Figure 4 their relative asphericities, acylindricities, and components of the diagonalized tensor of inertia together with the values corresponding to the model molecules mentioned before. Inspection of Figure 4 reveals that, in both representations, most dendrimers are grouped in couples. Thus, **A0** and **MA1** are structurally similar to each other,

(32) For recent studies on MD simulation on dendrimers, see for example: (a) Naidoo, K. J.; Hughes, S. J.; Moss, J. R. *Macromolecules* **1999**, *32*, 331. (b) Teobaldi, G.; Zerbetto, F. *J. Am. Chem. Soc.* **2003**, *125*, 7388. (c) Karatajos, K.; Adolf, D. B.; Davies, G. R. *J. Chem. Phys.* **2001**, *115*, 5310. (d) Lee, I.; Athey, B. D.; Wetzel, A. W.; Meixner, W.; Baker, J. R., Jr. *Macromolecules* **2002**, *35*, 4510.

(33) Field, M. J. *A Practical Introduction to the Simulation of Molecular Systems*; Cambridge University Press: Cambridge, 1999.

(34) Mattice, W. L. In *Dendritic Molecules: Concepts, Syntheses, Perspectives*; Newkome, G. R.; Moorefield, C. N.; Vögtle, F., Eds.; VCH: Weinheim, Germany, 1996; pp 1−36.

(35) Theodorov, D. N.; Suter, U. W. *Macromolecules* **1985**, *18*, 1206.

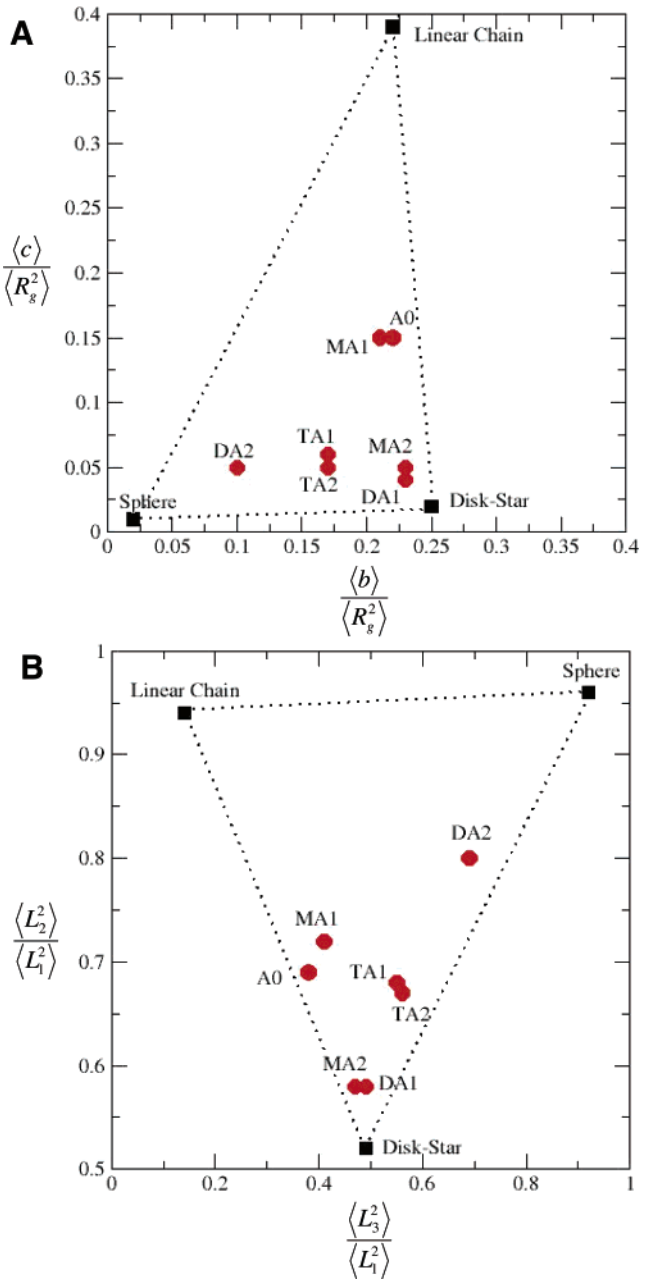

Figure 4. A) Representation of averaged asphericities $\langle b \rangle$ and acylindricities $\langle c \rangle$ relative to the averaged square of the radius of gyration $\langle R_g^2 \rangle$ for the different catalysts with respect to model spheric, linear chain, and disk-star reference molecules. (B) Same representation but considering the relative averaged $\langle L_i^2 \rangle$ components of the diagonalized tensor of inertia with respect to the largest one $\langle L_1^2 \rangle$.

occupying a halfway position between the linear chain and the disk-star structure. Similarly, **DA1** and **MA2** exhibit similar shapes, very similar to the disk-star geometry. Finally, the structural parameters of **TA1** and **TA2** are between those corresponding to the disk-star geometry and the sphere. Quite surprisingly, the structure most similar to the spheric shape is **DA2**, which must be related to the larger conformational freedom of this dendrimer. In summary, our results show that the dendrimers prepared cover a wide range of shapes, including structures similar to disk-star geometries as well as other dendrimers with different degrees of asphericity and acylindricity.

Correlation between Geometric Features and Catalytic Properties. The next step in our study was to find a correlation between structural properties of dendrimers **A0**, **MA1-2**, **DA1-2**, and **TA1-2** and the observed rate coefficients in the catalysis of the nitroaldol reaction depicted in Scheme 4. With this purpose, we have adapted the hard-sphere collision theory[36] to the structurally more complex dendrimers.

According to this theory, the kinetic constant k_{coll} associated with the collision of two reagents to give a chemical transformation is given by

$$k_{coll} = \sigma^* \left(\frac{8kT}{\pi\mu}\right)^{1/2} N_A \exp(-\Delta E_a/RT) \qquad (13)$$

where σ^* is the reactive collision cross section which can be expressed as

$$\sigma^* = P\sigma \qquad (14)$$

with P being the steric factor and σ the spheric collision cross section.

In eq 13, μ is the reduced mass of the reactants described by eq 15:

$$\mu = \frac{m_1 m_2}{m_1 + m_2} \qquad (15)$$

and ΔE_a is the activation energy, the remaining symbols of eq 13 having their usual meaning.

The crucial point to evaluate k_{coll} by means of eq 13 is the calculation of σ^*. One possible estimate is to assume that σ is linearly related to the average solvent accessible surface $\langle S_{AS} \rangle$. As the probe radius we have selected the average Csp^3-H distance of 1.10 Å, since this is the bond to be broken as a consequence of the effective collision of the nitroalkane and the catalyst. In Figure 5 we report the evolution of S_{AS} along the production time for all the catalysts, as well as one representation of this surface for dendrimer **TA2**.[37] In addition, for a given family of structurally related catalyst, P can be taken as inversely proportional to the molecular weight M_w of the catalyst. Therefore, for the dendrimers described above, the reactive cross section σ^* can be approximated as

$$\sigma^* = \alpha n_a \frac{\langle S_{AS} \rangle}{M_w} \qquad (16)$$

where n_a stands for the number of active sites, α being a proportionality constant. In our series of dendrimers, $n_a = 1$ for all catalysts.

If the catalytic centers of the dendrimers (the amino groups) have similar ability to abstract the proton of the nitroalkane molecule, the activation energy would be very similar. Under these conditions, the effective collision will be determined by the reactive cross section. Therefore, if the zeroth superscript denotes the parameter of amine **A0**, the relative kinetic constant of a given dendrimer with respect to **A0** can be approximated as

$$\frac{k_{coll}}{k^\circ_{coll}} \approx \frac{\langle S_{AS} \rangle M^\circ_w}{\langle S^\circ_{AS} \rangle M_w} \left(\frac{\mu^\circ}{\mu}\right)^{1/2} \qquad (17)$$

where the M_w and $\langle S_{AS} \rangle$ values can be taken from the data included in Table 2.

Table 2. Molecular Weights (M_w, Da), Averaged Squares of Radius of Gyration ($\langle R_g^2 \rangle$, Å^2), Maximum Radii ($\langle R_{Max} \rangle$, Å), Normalized Asphericities ($\langle b \rangle / \langle R_g^2 \rangle$) and Acylindricities ($\langle c \rangle / \langle R_g^2 \rangle$), Ratios of Principal Moments of the Gyration Tensor ($\langle L_i^2 \rangle / \langle L_1^2 \rangle$), and Solvent Accessible Surfaces[a] ($\langle S_{AS} \rangle$, Å^2) of Dendrimers **A0**, **MA1-2**, **DA1-2**, and **TA1-2**[b]

dendrimer	M_w	$\langle R_g^2 \rangle$	$\langle R_{max} \rangle$	$\langle b \rangle / \langle R_g^2 \rangle$	$\langle c \rangle / \langle R_g^2 \rangle$	$\langle L_3^2 \rangle / \langle L_1^2 \rangle$	$\langle L_2^2 \rangle / \langle L_1^2 \rangle$	$\langle S_{AS} \rangle$
A0	419.56	52.77	8.86	0.22	0.15	0.38	0.69	729.79
MA1	737.93	119.76	14.68	0.21	0.15	0.41	0.72	1189.88
MA2	1056.30	277.45	21.04	0.23	0.05	0.47	0.58	1684.96
DA1	1056.30	145.41	14.07	0.23	0.04	0.49	0.58	1668.99
DA2	2329.75	250.34	19.25	0.10	0.05	0.69	0.80	3456.70
TA1	1373.62	169.06	14.88	0.17	0.06	0.55	0.68	2017.85
TA2	4239.29	375.52	21.83	0.17	0.05	0.56	0.67	5738.21

[a] Computed with a probe radius of 1.1 Å. [b] All magnitudes were computed according to eqs 6−12; see text.

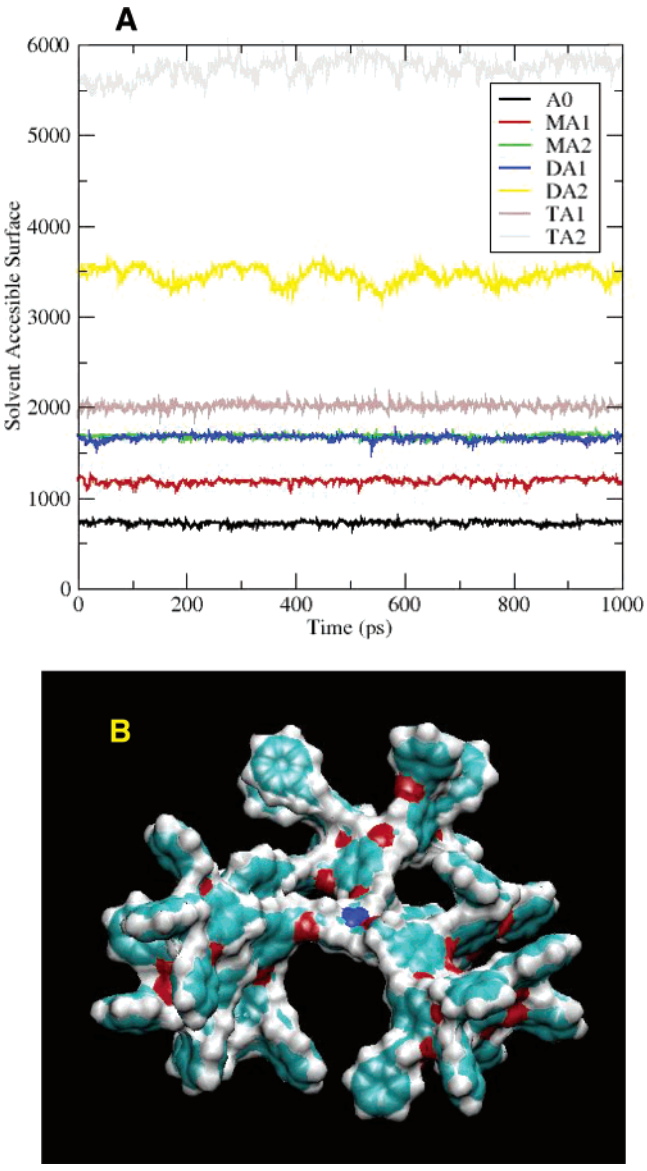

Figure 5. (A) Solvent accessible surfaces (S_{AS}, in Å^2, with a probe radius of 1.1 Å; see text) of catalysts **A0**, **MA1-2**, **DA1-2**, and **TA1-2** along the production time during the molecular dynamics simulations. (B) One view of the solvent accessible surface of dendrimer **TA2** with a probe radius of 1.1 Å. Regions occupied by nitrogen, oxygen, carbon, and hydrogen atoms are represented in blue, red, light blue, and white, respectively.

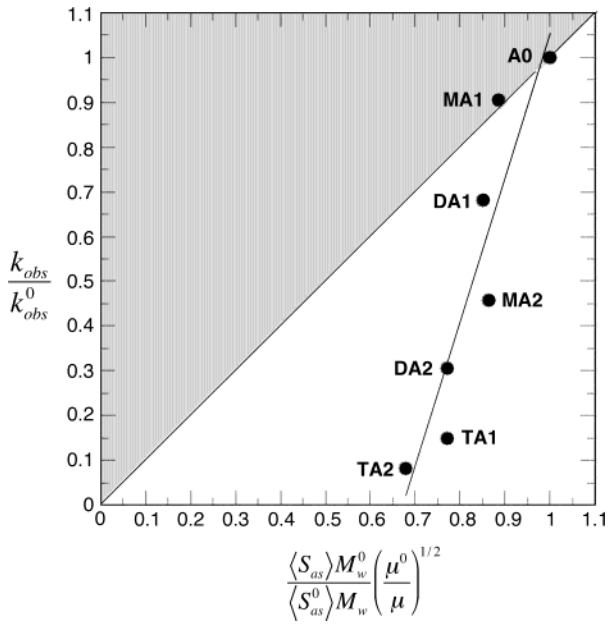

Figure 6. Relative rate coefficients(k_{obs}/k°_{obs}) versus parameters of amines **A0**, **MA1-2**, **DA1-2**, and **TA1-2**. Kinetic parameters correspond to the reaction between benzaldehyde and nitroethanol. The 45° line corresponds to the behavior described by eq 17. $\langle S_{AS} \rangle$, M_W, and μ stand for the averaged solvent accessible surface of the catalysts (with probe radius of 1.1 Å), molecular weight of the catalysts, and the reduced mass of the catalysts and nitroethanol, respectively. The zero superscript corresponds to amine **A0**. Gray and white colors indicate regions occupied by cooperative and noncooperative dendrimers, respectively (see text).

In Figure 6 we have represented the relative parameters included in eq 17 versus the experimentally observed kinetic parameters k_{obs} (vide supra). We have found that there is a linear departure from the behavior described by eq 17. Therefore, we can write the following expression:

$$\frac{k_{obs}}{k^\circ_{obs}} = \phi \frac{\langle S_{AS} \rangle M^\circ_w}{\langle S^\circ_{AS} \rangle M_w} \left(\frac{\mu^\circ}{\mu} \right)^{1/2} + \theta \qquad (18)$$

with $\phi = 3.8$ and $\theta = -2.2$, the regression factor being $r^2 = 0.921$. It is noteworthy that the catalytic behavior of the smallest molecule **MA1** is described by eq 17, whereas the departure from this behavior is larger as the generation number and/or the branching index increases. Therefore, we can describe the behavior of an ensemble of structurally related catalytic dendrimers in terms of a sole parameter. Although further studies should test if the model presented here is general, we can anticipate that noncooperative catalytic dendrimers will lie in the region colored in white in Figure 6, whereas cooperative

(36) (a) Atkins, P. W. *Physical Chemistry*; Oxford University Press: Oxford, 1998; pp 820−825. (b) Berry, R. S.; Rice, S. A.; Ross, J. *Physical Chemistry*; Oxford University Press: New York, 2000; pp 906−910.
(37) The graphic representations of the solvent accessible surfaces were obtained by means of the Visual Molecular Dynamics program. See: Umpherey, W.; Dalke, A.; Schulten, K. *J. Mol. Graphics* **1996**, *14*, 33.

dendrimers will exhibit a behavior not reducible to eqs 17 or 18 and will lie in the region marked in gray in the figure. Therefore, the models reported in this article can be used as a general criterion to measure the relative catalytic power of different types of dendrimers.

Conclusions

From the results reported in this article the following conclusions can be drawn. (i) Dendrimers with one active site at the core and with shapes varying from linear to spheric can exhibit catalytic power, which decreases as the generation number and/or the degree of branching increases, provided that the dendritic regions do not participate in the chemical transformation under consideration. (ii) In this kind of noncooperative dendrimers and, at least in the case studied, the impact of the shape of the dendrimer on the stereochemical outcome is low to negligible. (iii) For the reaction studied in this article, there is a linear correlation between the rate coefficient and a combined parameter derived from the solvent accessible surface, the molecular weight, and the reduced mass. The slope of the linear regression thus obtained can be used to measure the effectiveness and the cooperative effects in different types of structurally related catalytic dendrimers.

Experimental Section

General Method for the Preparation of Catalytic Amines. A solution of triethanolamine (0.47 g, 3.15 mmol) in dry THF (10 mL) under argon atmosphere was cooled with an ice/water bath. NaH (0.40 g, 10.0 mmol) was added, and the suspension was stirred for 10 min. A solution of the corresponding bromide (10.0 mmol) in dry THF (30 mL) and dry DMF (10 mL) was slowly added, and the mixture was stirred at room temperature. After completion of the reaction, Et_2O (60 mL) was added, and the organic layer was washed with H_2O (3×25 mL), dried over Na_2SO_4, and evaporated under reduced pressure. The crude products were purified by column chromatography with ethyl acetate as eluent, yielding the amines as syrups that were fully characterized.

A0: 61% yield. ^{1}H NMR (δ, ppm, $CDCl_3$): 7.31−7.28 (m, 15H), 4.48 (s, 6H), 3.55 (t, $J = 6.0$ Hz, 6H), 2.84 (t, $J = 6.0$ Hz, 6H). ^{13}C NMR (δ, ppm, $CDCl_3$): 138.3, 128.2, 127.5, 127.4, 73.0, 68.7, 54.5. Anal. Calcd for $C_{27}H_{33}NO_3$: C, 77.28; H, 7.94; N, 3.34. Found: C, 77.26; H, 7.91; N, 3.36. MS calcd for $C_{27}H_{33}NO_3$: 419.25; found (MALDI-TOF): m/z 420.25 $[M + H]^+$.

MA1: 75% yield. ^{1}H NMR (δ, ppm, $CDCl_3$): 7.41−7.28 (m, 15H), 7.21 (d, $J = 2.1$ Hz, 6H), 6.90 (d, $J = 2.1$ Hz, 6H), 5.05 (s, 6H), 4.45 (s, 6H), 3.55 (t, $J = 5.54$ Hz, 6H), 2.85 (t, $J = 5.54$ Hz, 6H). ^{13}C NMR (δ, ppm, $CDCl_3$): 159.6, 137.3, 132.6, 129.2, 128.5, 127.9, 127.4, 115.1, 72.8, 70.0, 69.7, 54.6. Anal. Calcd for $C_{48}H_{51}NO_6$: C, 78.11; H, 6.98; N, 1.89. Found: C, 77.80; H, 7.02; N, 1.90. MS calcd for $C_{48}H_{51}NO_6$: 737.37; found (MALDI-TOF): m/z 738.32 $[M + H]^+$.

MA2: 53% yield. ^{1}H NMR (δ, ppm, $CDCl_3$): 7.42−7.18 (m, 27H), 7.02−6.87 (m, 12H), 5.06 (s, 6H), 4.95 (s, 6H), 4.42 (s, 6H), 3.57 (t, $J = 5.6$ Hz, 6H), 2.84 (t, $J = 5.6$ Hz, 6H). ^{13}C NMR (δ, ppm, $CDCl_3$): 159.5, 137.0, 131.1, 129.2, 129.1, 128.5, 127.9, 127.4, 114.9, 114.7, 72.7, 70.0, 69.7, 54.5. Anal. Calcd for $C_{69}H_{69}NO_9$: C, 78.44; H, 6.59; N, 1.33. Found: C, 79.03; H, 6.55; N, 1.31. MS calcd for $C_{69}H_{69}NO_9$: 1055.50; found (MALDI-TOF): m/z 1056.62 $[M + H]^+$.

DA1: 70% yield. ^{1}H NMR (δ, ppm, $CDCl_3$): 7.41−7.29 (m, 30H), 6.58 (d, $J = 2.2$ Hz, 6H), 6.50 (t, $J = 2.2$ Hz, 3H), 4.95 (s, 12H), 4.41 (s, 6H), 3.55 (t, $J = 6.5$ Hz, 6H), 2.81 (t, $J = 6.5$ Hz, 6H). ^{13}C NMR (δ, ppm, $CDCl_3$): 159.8, 140.8, 136.7, 128.3, 127.7, 127.3, 106.2, 101.0, 72.7, 69.7, 68.6, 54.5. Anal. Calcd for $C_{69}H_{69}NO_9$: C, 78.44; H, 6.59; N, 1.33. Found: C, 78.07; H, 6.55; N, 1.34. MS calcd for $C_{69}H_{69}NO_9$: 1055.50; found (MALDI-TOF): m/z 1056.68 $[M + H]^+$.

DA2: 50% yield. ^{1}H NMR (δ, ppm, $CDCl_3$): 7.40−7.20 (m, 60H), 6.67 (d, $J = 2.2$ Hz, 12H), 6.59 (d, $J = 2.2$ Hz, 6H), 6.57 (t, $J = 2.2$ Hz, 6H), 6.52 (t, $J = 2.2$ Hz, 3H), 5.05 (s, 24H), 4.90 (s, 12H), 4.37 (s, 6H), 3.50 (t, $J = 6.1$ Hz, 6H), 2.76 (t, $J = 6.1$ Hz, 6H). ^{13}C NMR (δ, ppm, $CDCl_3$): 160.0, 159.8, 140.9, 139.2, 136.7, 128.4, 127.9, 127.5, 106.2, 101.4, 101.1, 72.9, 69.9, 69.7, 68.7, 54.7. Anal. Calcd for $C_{153}H_{141}NO_{21}$: C, 78.86; H, 6.11; N, 0.60. Found: C, 79.05; H, 6.07; N, 0.59. MS calcd for $C_{153}H_{141}NO_{21}$: 2329.75; found (MALDI-TOF): m/z 2330.89 $[M + H]^+$.

TA1: 79% yield. ^{1}H NMR (δ, ppm, $CDCl_3$): 7.41−7.21 (m, 45H), 6.52 (s, 6H), 5.04 (s, 12H), 4.98 (s, 6H), 4.41 (s, 6H), 3.52 (t, $J = 5.3$ Hz, 6H), 2.84 (t, $J = 5.3$ Hz, 6H). ^{13}C NMR (δ, ppm, $CDCl_3$): 152.9, 137.9, 137.1, 134.1, 128.5, 128.4, 128.1, 127.8, 127.7, 127.4, 107.1, 75.2, 73.1, 71.1, 68.8, 54.7. Anal. Calcd for $C_{90}H_{87}NO_{12}$: C, 78.62; H, 6.39; N, 1.02. Found: C, 78.40; H, 6.42; N, 1.00. MS calcd for $C_{90}H_{87}NO_{12}$: 1373.62; found (MALDI-TOF): m/z 1374.33 $[M + H]^+$.

TA2: 27% yield. ^{1}H NMR (δ, ppm, $CDCl_3$): 7.32−7.07 (m, 135H), 6.74 (s, 6H), 6.70 (s, 12H), 6.63 (s, 6H), 4.89 (s, 54H), 4.80 (s, 6H), 4.74 (s, 12H), 4.38 (s, 6H), 3.56 (t, $J = 5.8$ Hz, 6H), 2.86 (t, $J = 5.8$ Hz, 6H). ^{13}C NMR (δ, ppm, $CDCl_3$): 152.9, 138.0, 137.8, 136.8, 134.4, 133.4, 132.6, 128.3, 128.2, 128.0, 127.7, 127.6, 127.4, 107.5, 106.7, 75.1, 73.0, 71.4, 71.0, 70.8, 69.0, 54.8. Anal. Calcd for $C_{279}H_{249}NO_{39}$: C, 79.02; H, 5.93; N, 0.33. Found: C, 78.89; H, 6.01; N, 0.34. MS calcd for $C_{279}H_{249}NO_{39}$: 4239.29; found (MALDI-TOF): m/z 4240.77 $[M + H]^+$.

Procedure for the Kinetic Experiments. To a mixture of freshly purified and distilled benzaldehyde[38] (0.051 mL, 0.5 mmol), 2-nitroethanol (0.359 mL, 5.0 mmol), and benzonitrile (0.051 mL, 0.5 mmol), the corresponding catalyst (7.5×10^{-3} mmol) was added at 25 °C. At certain times (see the Supporting Information for additional details), aliquots were withdrawn with a micropipet, placed on a KBr disk, and immediately analyzed by IR spectroscopy. The decay of the C═O st. band (1724−1672 cm^{-1}) of the starting aldehyde was monitored with respect to the internal standard (benzonitrile, C≡N st. band, 2266−2200 cm^{-1}). At the end of each experiment, the diastereomeric ratio of the products was calculated by ^{1}H NMR spectroscopy on crude reaction mixtures, according to literature spectroscopic data.[25]

Acknowledgment. We thank the Ministerio de Ciencia y Tecnología of Spain (Project BQU2001-0904) and the Gobierno Vasco-Eusko Jaurlaritza (Grant 9/UPV 00170.215-13548/2001) for financial support. A.Z. also thanks the Gobierno Vasco-Eusko Jaurlaritza for a grant.

Supporting Information Available: Full experimental details and characterization of bromides **2**, **3**, **4**, **5**, **6**, and **7** and their precursor alcohols and esters, kinetic measurements, ratios of averaged principal moments of the radius of gyration tensor, relative asphericities, and acylindricities of reference molecules hexamethyl benzene, *n*-pentane, and neopentane (PDF). This material is available free of charge via the Internet at http://pubs.acs.org.

JA039888S

(38) Armarego, W. L. F.; Perrin, D. D. *Purification of Laboratory Chemicals*; Butterworth-Heinemann: Oxford, 1996; p 99.